The Astrophysical Journal, 872:38 (8pp), 2019 February 10 https://doi.org/10.3847/1538-4357/aafe10

Laboratory Photochemistry of Covalently Bonded Fluorene Clusters: Observation of an Interesting PAH Bowl-forming Mechanism

Weiwei Zhang[1,2,7], Yubing Si[3], Junfeng Zhen[1,2], Tao Chen[4,6], Harold Linnartz[5], and Alexander G. G. M. Tielens[6]
[1] CAS Key Laboratory for Research in Galaxies and Cosmology, Department of Astronomy, University of Science and Technology of China, Hefei 230026, People's Republic of China; jfzhen@ustc.edu.cn
[2] School of Astronomy and Space Science, University of Science and Technology of China, Hefei 230026, People's Republic of China
[3] Henan Provincial Key Laboratory of Nanocomposites and Applications, Institute of Nanostructured Functional Materials, Huanghe Science and Technology College, Zhengzhou 450006, People's Republic of China
[4] School of Engineering Sciences in Chemistry, Biotechnology and Health, Department of Theoretical Chemistry & Biology, Royal Institute of Technology, SE-10691, Stockholm, Sweden
[5] Sackler Laboratory for Astrophysics, Leiden Observatory, Leiden University, P.O. Box 9513, 2300 RA Leiden, The Netherlands
[6] Leiden Observatory, Leiden University, P.O. Box 9513, 2300 RA Leiden, The Netherlands
Received 2018 July 30; revised 2019 January 7; accepted 2019 January 8; published 2019 February 8

Abstract

The fullerene C_{60}, one of the largest molecules identified in the interstellar medium (ISM), has been proposed to form top-down through the photochemical processing of large (more than 60 C atoms) polycyclic aromatic hydrocarbon (PAH) molecules. In this article, we focus on the opposite process, investigating the possibility that fullerenes form from small PAHs, in which bowl-forming plays a central role. We combine laboratory experiments and quantum chemical calculations to study the formation of larger PAHs from charged fluorene clusters. The experiments show that with visible laser irradiation, the fluorene dimer cation—$[C_{13}H_9{-}C_{13}H_9]^+$—and the fluorene trimer cation—$[C_{13}H_9{-}C_{13}H_8{-}C_{13}H_9]^+$—undergo photodehydrogenation and photoisomerization, resulting in bowl-structured aromatic cluster ions, $C_{26}H_{12}^+$ and $C_{39}H_{20}^+$, respectively. To study the details of this chemical process, we employ quantum chemistry that allows us to determine the structures of the newly formed cluster ions, to calculate the dissociation energies for hydrogen loss, and to derive the underlying reaction pathways. These results demonstrate that smaller PAH clusters (with less than 60 C atoms) can convert to larger bowled geometries that might act as building blocks for fullerenes, because the bowl-forming mechanism greatly facilitates the conversion from dehydrogenated PAHs to cages. Moreover, the bowl-forming induces a permanent dipole moment that—in principle—allows one to search for such species using radio astronomy.

Key words: astrochemistry – ISM: molecules – methods: laboratory: molecular – molecular processes – ultraviolet: ISM

1. Introduction

Progress in observational techniques, both ground-based and from space missions, shows that molecular complexity in space may be beyond our imagination. Fullerenes, such as C_{60}, are seen in very different environments and thought to be chemically linked to polycyclic aromatic hydrocarbon (PAH) molecules, as discussed in Tielens (2013). Interstellar PAHs and PAH derivatives (e.g., PAH clusters) are believed to be ubiquitous in the interstellar medium (ISM), where they are generally thought to be responsible for the strong mid-infrared (IR) features in the 3–17 μm range that dominate the spectra of most Galactic and extragalactic sources (Allamandola et al. 1989; Puget & Leger 1989; Sellgren 1984; Genzel et al. 1998). PAH cations have been proposed as carriers of the diffuse interstellar bands (DIBs) (Salama et al. 1996; Gredel et al. 2011). IR spectra of circumstellar and interstellar sources have revealed the presence of the fullerenes C_{60} and C_{70} in space (Cami et al. 2010; Sellgren et al. 2010). Recently, several DIBs around 1 μm have been linked to electronic transitions of C_{60}^+ (Campbell et al. 2015; Walker et al. 2015; Cordiner et al. 2017). Hence, understanding the formation and destruction processes of PAHs and fullerenes has attracted much attention in the field of molecular astrophysics (Tielens 2013).

Based on IR observations of interstellar reflection nebulae, Berné et al. proposed that PAHs can be converted into graphene and subsequently to C_{60} by photochemical processing combining the effects of dehydrogenation, fragmentation, and isomerization (Berné & Tielens 2012; Berné et al. 2015). This idea is supported by laboratory studies, which demonstrate that $C_{66}H_{22}^+$ can be transformed into C_{60}^+ upon irradiation, following full dehydrogenation, graphene flake-folding, and C_2-losing chemical pathways (Zhen et al. 2014a). The conversion of graphene flakes to cages and fullerenes has been studied using transmission electron microscopy and quantum chemistry (Chuvilin et al. 2010). Pietrucci & Andreoni (2014) have elucidated relevant reaction routes and molecular intermediaries in the conversion of graphene flakes into cages and fullerenes.

The photochemical breakdown of PAHs to smaller hydrocarbons and the conversion to fullerenes may be counteracted by a PAH growth process that converts clusters of small PAHs into larger, fully aromatic PAHs. Such a process could start with the formation of van der Waals-bonded or charge transfer-bonded PAHs clusters that are photochemically converted into large PAHs and PAH cations (Zhen et al. 2018). The presence of PAH clusters in the deeper zones of photodissociation

[7] Current address: Department of Mechanical and Nuclear Engineering, Pennsylvania State University, University Park, PA 16802, USA.

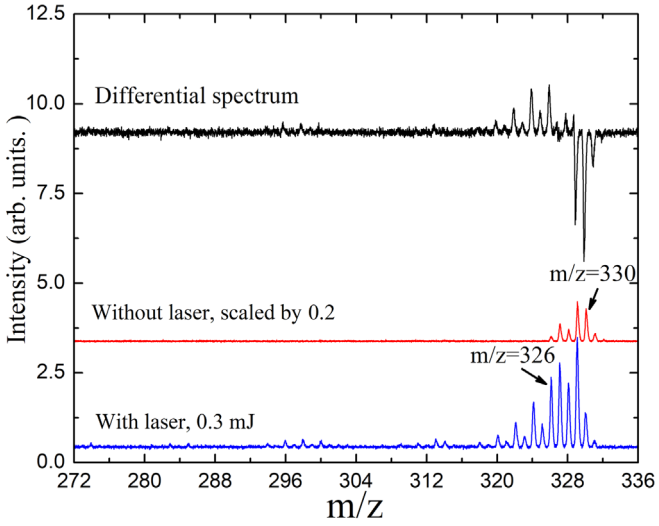

Figure 1. Mass spectrum of fluorene dimer cluster cations (e.g., $C_{26}H_{18}^{+}$, $m/z = 330$) without irradiation (red), irradiated at 595 nm (blue), and the differential spectrum (black).

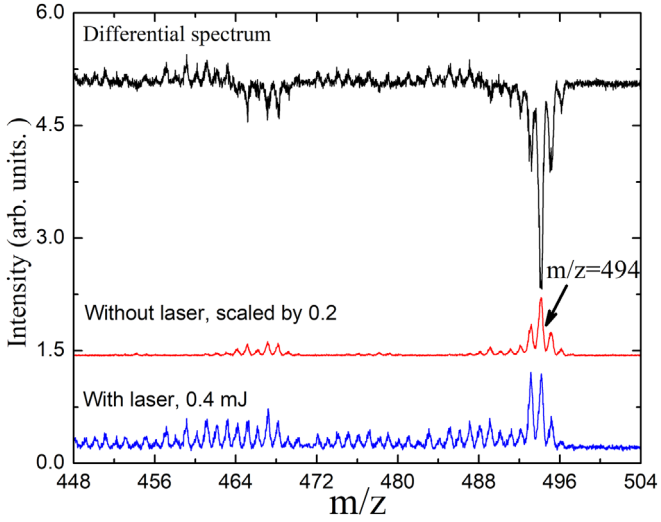

Figure 2. Mass spectrum of fluorene trimer cluster cations (e.g., $C_{39}H_{26}^{+}$, $m/z = 494$) without irradiation (red), irradiated at 595 nm (blue), and the differential spectrum (black).

regions (PDRs) has been inferred from singular value decomposition analysis of *ISO* and *Spitzer* spectral maps of PDRs (Rapacioli et al. 2005; Berné et al. 2007). Rhee et al. (2007), on the other hand, suggest that PAH clusters are present near the surfaces of PDRs. Their suggestion is based upon a putative association of the extended red emission (Vijh et al. 2004) with luminescence by charged PAH clusters. The formation and destruction of PAH clusters has been studied by Rapacioli et al. (2006). In their analysis, these authors balanced coagulation with UV-driven photoevaporation of weakly bonded van der Waals clusters. However, rather than thermal evaporation, photochemical evolution of van der Waals clusters may result in the formation of covalent bonds. Experimental and ab initio molecular dynamics studies on ionization of van der Waals-bonded acetylene clusters reveal a reaction channel toward the benzene cation. In this route, the excess photon and chemical energy is taken away by an H atom or by one of the spectator acetylenes in the cluster (Stein et al. 2017). Similar, UV-driven reaction routes may exist for PAH clusters, resulting in covalently bonded PAH dimers, trimers, or larger multimers. The presence of aromatic structures bonded by aliphatic links in space has also been postulated by Micelotta et al. (2012) as an explanation for spectral detail of the aromatic infrared bands. In addition, the driving force of cluster growth in the formation process of soot nuclei is the generation of the PAH radical, which is formed by releasing hydrogen atoms from PAHs. Afterwards, the reaction between PAH radicals and PAHs leads to covalently bonded clusters (Le Page et al. 2001; Richter & Howard 2000; Richter et al. 2005). Finally, we point toward experimental studies on the interaction of energetic ions with PAH clusters, which also lead to covalently bonded PAH multimers (Zettergren et al. 2013; Gatchell et al. 2015; Gatchell & Zettergren 2016).

In our experimental set-up, we have identified an efficient clustering method that naturally leads to covalently bonded dimer and trimer cations. In an earlier study, we reported the photochemical conversion of such pyrene clusters into large, fully aromatic PAHs (Zhen et al. 2018). Here, we extend these studies to fluorene clusters and demonstrate that the resulting molecules incorporate pentagons. The inclusion of pentagons in the molecular structure leads to curvature of the species. We have selected fluorene ($C_{13}H_{10}$) as a prototypical molecule for its unique molecular property: a carbon skeleton, in which two six-membered rings are fused to a central pentagonal ring. While its abundance in the ISM is unknown, fluorene has been detected in carbonaceous meteorites (Sephton 2002). In addition, fluorene is very amenable to experimental studies because of its small size. It is likely that interstellar PAH clusters consist of PAHs that are much larger than fluorene. Nevertheless, the photochemical behavior of fluorene identifies a number of key processes that may play a role in the evolution of PAH clusters in space. Specifically, our results show that bowl-forming is an important aspect of the photochemical evolution of PAHs, and this can be a first step in the formation of cages and fullerenes.

As our experiments are not optimized to study the formation of covalently bonded clusters, we focus here exclusively on their subsequent evolution under irradiation. Further studies such as the acetylene studies (Stein et al. 2017) are required to address the kinetics of the formation of such clusters. Together with our experiment, such kinetic parameters will be necessary to evaluate the abundance of covalently bonded PAH clusters and their role in space.

2. Experimental Methods

The experiments have been performed on i-PoP, our instrument for photodissociation of PAHs, a high vacuum ion trap time-of-flight (TOF) system that has been described in detail in Zhen et al. (2014b). In short, neutral fluorene (Aldrich, 98%) species are transferred into the gas phase from an oven (~305 K). The fluorene molecules are ionized by an electron gun. A steel mesh (hole diameter ~0.1 mm) is put on top of the oven to increase the local density of fluorene molecules to facilitate cluster formation. The increased density in the fluorene plume allows the formation of cation clusters as discussed in Zhen et al. (2018). In our experiments, the low energy barrier for H loss from fluorene (2.3 eV, West et al. 2018) leads to efficient radical formation upon electron gun

irradiation and promotes the formation of covalently bonded clusters. Once formed, cation species are transported into a quadrupole ion trap and trapped. The trapped ions are then irradiated by several (typically ~5) pulses from a pulsed Nd:YAG pumped dye laser system, providing visible light (with wavelengths around 595 nm, linewidth ~0.2 cm^{-1}, pulse duration ~5 ns). After irradiation the trap is opened and dissociation products are measured using the TOF mass spectrometer.

3. Experimental Results and Discussion

Typical TOF mass spectra of the fluorene dimer and trimer cations are shown in Figures 1 and 2, respectively. In the sample condition without laser irradiation (Figure 1, middle panel), several peaks, corresponding to different species, are observed for the fluorene dimer cation, i.e., these species are the direct result of electron impact ionization. In order to interpret these mass peaks correctly, it is important to note that the chance of producing a ^{13}C-containing cluster increases with the number of C atoms involved. The method to discriminate between pure ^{12}C and ^{13}C-polluted mass signals has been described in our previous studies (Zhen et al. 2014b). After correction for the ^{13}C isotope and normalization, we conclude that six dimer species are formed at this stage, namely $C_{26}H_{19}^+$ (0.2%), $C_{26}H_{18}^+$ (26.5%), $C_{26}H_{17}^+$ (41.6%), $C_{26}H_{16}^+$ (7.1%), $C_{26}H_{15}^+$ (19.6%), and $C_{26}H_{14}^+$ (5.0%). We emphasize that this procedure leads exclusively to dehydrogenated fluorene dimers. It is tempting to speculate that any (ionized) cluster that did not make a covalent bond and is bonded solely by weak van der Waals bonds will rapidly evaporate before or in the trap due to the excess internal energy.

Upon laser irradiation (Figure 1, lower panel, 0.3 mJ), many new peaks are observed in the mass spectrum (Figure 1, upper panel, differential spectrum). The dehydrogenation sequence differs from that observed for monomers such as hexa-peri-hexabenzocoronene ($C_{42}H_{18}$, HBC, Zhen et al. 2014b). The fragmentation pattern of HBC is characterized by even-H peaks stronger than odd-H peaks. In contrast, in the fragmentation pattern of the fluorene dimers, two short but different dehydrogenation sequences can be distinguished in the ranges $m/z = 326-330$ and $m/z = 318-326$, respectively. In the range $m/z = 326-330$, the fraction of species with an odd number of hydrogens is higher than that with an even number, e.g., the intensity of $C_{26}H_{17}^+$ ($m/z = 329$) and $C_{26}H_{15}^+$ ($m/z = 327$) is stronger than that of their neighbor, $C_{26}H_{16}^+$ ($m/z = 328$). On the other hand, in the range $m/z = 318-326$, the dehydrogenation behavior is that of regular PAHs with stronger even peaks than odd peaks, e.g., the intensity of the $C_{26}H_{12}^+$ ($m/z = 324$) peak is stronger than that of its neighbors ($C_{26}H_{11}^+$, $m/z = 323$ and $C_{26}H_{13}^+$, $m/z = 325$). Following our study of the pyrene dimer, we suggest that the two different dehydrogenation patterns in these two m/z regions imply that the fluorene dimer cations (e.g., $[C_{13}H_9-C_{13}H_9]^+$ or $C_{26}H_{18}^+$) convert to aromatic species with more conjugated π-bonds (e.g., $C_{26}H_{12}^+$) after dehydrogenation. We will discuss details in the next section.

The typical mass spectrum of the fluorene trimer cluster cation is shown in Figure 2. Similar to the fluorene dimer mass region, without laser irradiation (Figure 2, middle panel), the dominant species are the partially dehydrogenated fluorene trimer cluster cations (e.g., $C_{39}H_{26}^+$ with $m/z = 494$). With laser irradiation (Figure 2, lower panel, 0.4 mJ), a wide range of fragment ions is evident in the mass spectrum (Figure 2, upper panel, differential spectrum). In this case no –H/–2H intensity alternations are found.

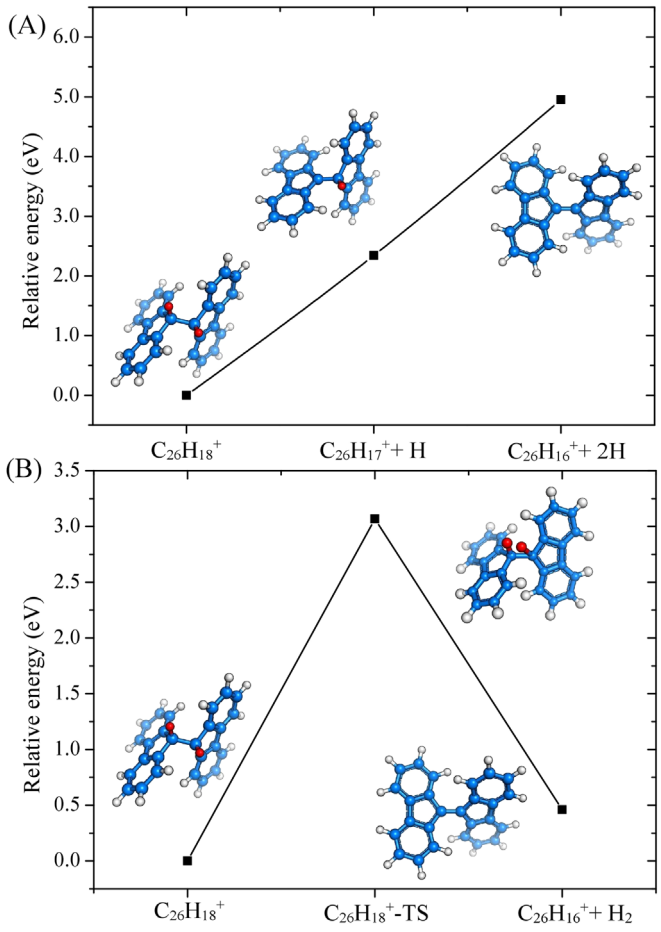

Figure 3. The reaction pathway of the fluorene dimer cluster cation: (A) from $C_{26}H_{18}^+$ to $C_{26}H_{16}^+$ with the H + H loss channel; (B) from $C_{26}H_{18}^+$ to $C_{26}H_{16}^+$ with the H_2 loss channel. Carbon is shown in blue, nonreactive hydrogen in gray, and abstracted hydrogen in red.

4. Results of the Theoretical Calculation and Discussion

We observed a series of m/z as shown in Figures 1 and 2, and we employ quantum chemistry to link these observations to their structures and identify possible reaction pathways. Peaks in a mass spectrum can refer to more than one isomer, so it is difficult to infer reaction products and pathways from the experiments alone. Therefore, the interpretation of experimental data is further investigated by density functional theory (DFT) calculations. We have used DFT to calculate the structure of the dominant fluorene dimer and trimer cations ($C_{26}H_{18}^+$ and $C_{39}H_{26}^+$). The calculations result in the optimized carbon skeletons shown in Figure 3 (see Appendix A for details).

Based on our calculations, the dimer dissociation process from $C_{26}H_{18}^+$ to $C_{26}H_{12}^+$ occurs in three steps. The first step (Figure 3(A)) is the dehydrogenation from $C_{26}H_{18}^+$ to $C_{26}H_{16}^+$, losing two hydrogen atoms one by one from the sp^3 hybridized carbon atoms of the fluorene dimer cation with a dissociation energy smaller than 3.0 eV (2.3 and 2.6 eV, respectively). Such a step-by-step dissociation of H atoms, from $C_{26}H_{18}^+$ ($m/z = 328$) to $C_{26}H_{17}^+$ ($m/z = 327$), and from

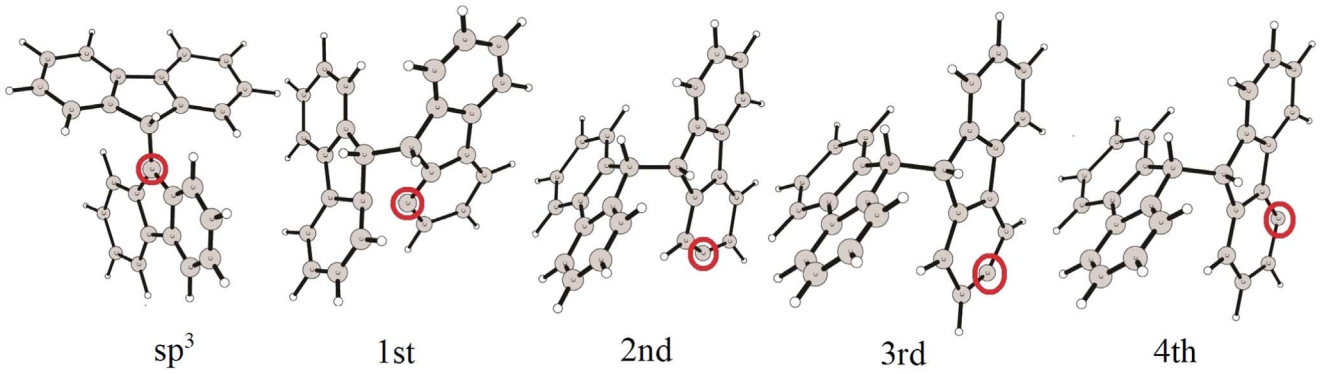

Figure 4. Possible positions in $C_{26}H_{18}^{+}$ from which an H atom has been lost are labeled here as sp^3, 1st, 2nd, 3rd, and 4th.

$C_{26}H_{17}^{+}$ to $C_{26}H_{16}^{+}$ (326), indicates that $C_{26}H_{17}^{+}$ acts as an intermediary (IM).

From our calculations, we conclude that dissociation of the C–H bond plays an important role in the polymerization process. We thus compared the dissociation energies for hydrogen from different positions (corresponding to $C_{26}H_{18}^{+}$ to $C_{26}H_{17}^{+}$), as shown in Figure 4. The DFT calculations show that the dissociation energies of hydrogen are 2.3, 3.5, 5.1, 5.0, and 5.0 eV from sp^3, first, second, third, and fourth positions, respectively. This indicates that losing a hydrogen atom from the sp^3 hybridized carbon atoms is much easier than losing an aromatic hydrogen. This is a common characteristic of mixed aromatic–aliphatic species (Jolibois et al. 2005; Chen et al. 2015; Trinquier et al. 2017; Castellanos et al. 2018; West et al. 2018). As such, theoretical calculations confirm that the pathway in Figure 3(A) (losing H from the sp^3 position) is energetically preferable.

In addition, for the first step, as shown in Figure 3, the two hydrogen atoms attached to sp^3 hybridized carbon atoms might be dissociated at the same time to form H_2 (see Figure 3(B)), rather than be lost one by one. We thus studied this H_2-releasing reaction pathway and found that the reaction barrier is 3.1 eV, which is much larger than the barrier for losing the first H atom (2.3 eV), as shown in Figure 3(A). We confirm that the $C_{26}H_{17}^{+}$ acts as an intermediary, in agreement with the experimental results (Figure 1).

The second step is illustrated in Figure 5(A). After losing these two hydrogen atoms, the C–C bond between the two fluorene monomers can rotate more freely with a small energy barrier, resulting in isomerization. As shown here, the reaction barrier for the isomerization process is only 1.8 eV, much lower than needed for a dehydrogenation step. At the same time, a cyclization process is observed by C–C bond formation to produce the intermediate structure, IM1a. As the six-membered carbon ring is formed, the additional H on the overcoordinated carbon (sp^3) atom is lost. Specifically, our calculation shows that the reaction barrier that must be overcome to lose the first hydrogen atom is only 1.45 eV (from IM1 to $C_{26}H_{15}^{+}$ + H), and it takes 1.8 eV for the second step (from $C_{26}H_{15}^{+}$ to $C_{26}H_{14}^{+}$ + H). The two-step dissociation process will generate $C_{26}H_{15}^{+}$, which is also reflected in the mass spectrum with high intensity. Our calculations demonstrate that both dehydrogenation processes are much faster than that in the first step from $C_{26}H_{18}^{+}$ to $C_{26}H_{16}^{+}$ due to their lower dissociation energies. During this step, the distorted fluorene dimer cation becomes a large planar PAH with 2 five- and 5 six-carbon rings. This mechanism shows many similarities to that recently

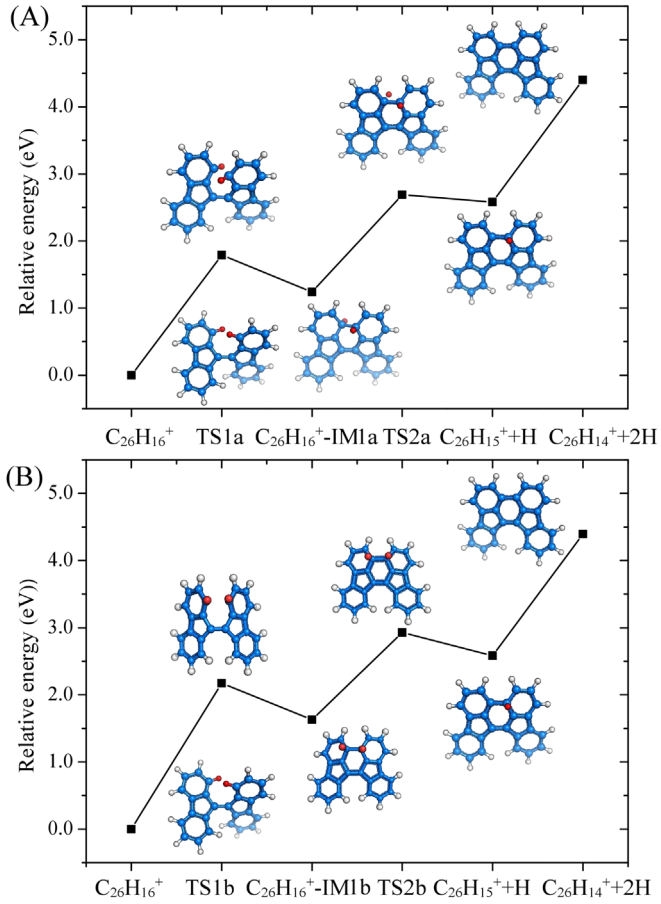

Figure 5. Reaction pathway of the fluorene dimer cluster cation: (A) from $C_{26}H_{16}^{+}$ to $C_{26}H_{14}^{+}$ with the H + H loss channel; (B) from $C_{26}H_{16}^{+}$ to $C_{26}H_{14}^{+}$ with the other H + H loss channel. Carbon is shown in blue, nonreactive hydrogen in gray, and abstracted hydrogen in red.

studied for the photochemistry of pyrene-based clusters (Zhen et al. 2018).

In the third step, two more hydrogen atoms are lost from $C_{26}H_{14}^{+}$ to produce $C_{26}H_{12}^{+}$ (Figure 6(A)). $C_{26}H_{14}^{+}$ isomerizes, overcoming the transition state (TS) with a barrier of 3.0 eV to form IM2a. Compared to the isomerization process in the second step, the barrier in this final step is much higher, because isomerization for a large planar PAH is more difficult than for a distorted one. In this isomerization step, the planar PAH is forced to form a bowl structure, composed of five- and six-membered carbon rings, which can be easily recognized as

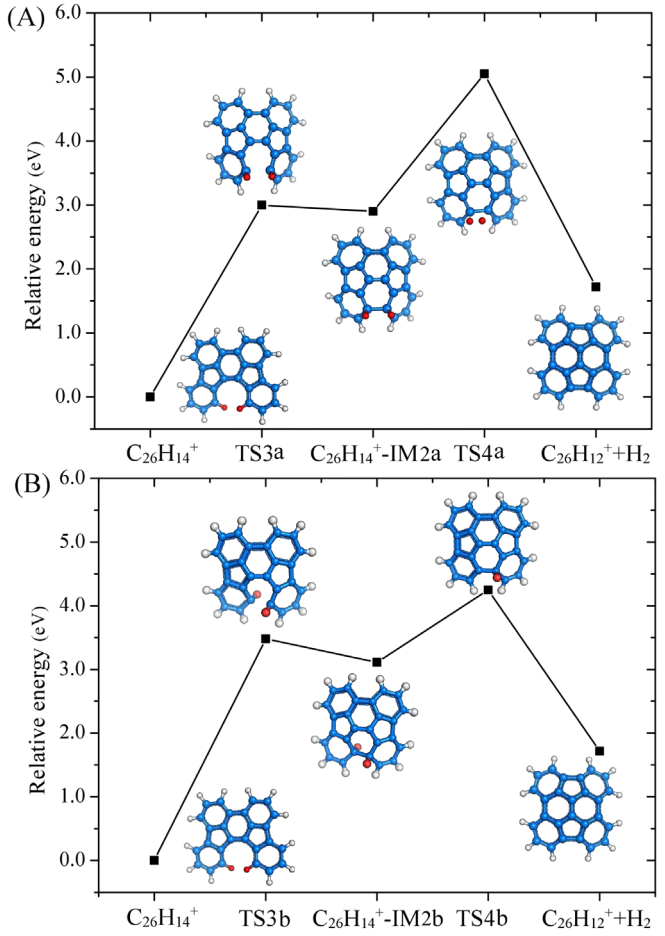

Figure 6. Reaction pathway of the fluorene dimer cluster cation: (A) from $C_{26}H_{14}^+$ to $C_{26}H_{12}^+$ with the H_2 loss channel; (B) from $C_{26}H_{14}^+$ to $C_{26}H_{12}^+$ with the H + H loss channel. Carbon is shown in blue, nonreactive hydrogen in gray, and abstracted hydrogen in red.

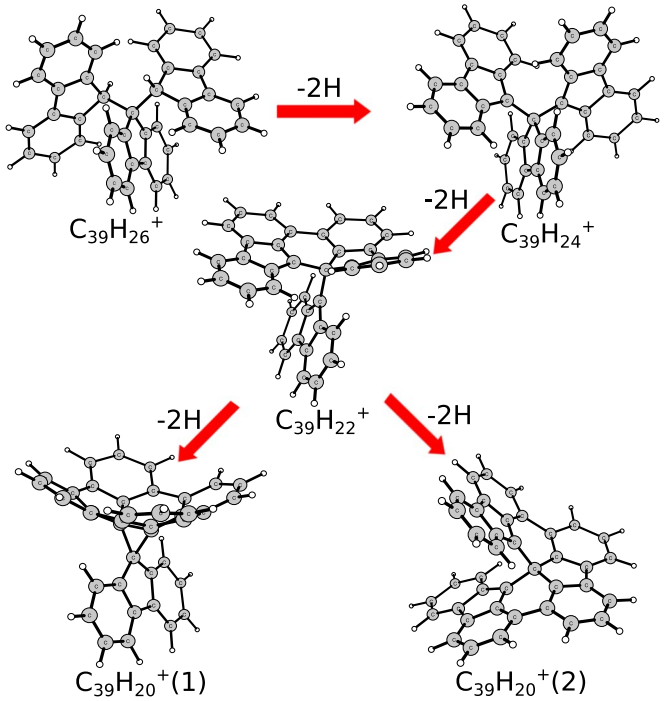

Figure 7. Dehydrogenation process of the fluorene trimer cluster cation: from $C_{39}H_{26}^+$, to $C_{39}H_{24}^+$, to $C_{39}H_{22}^+$, to $C_{39}H_{20}^+$. Carbon and hydrogen atoms are shown in gray and white, respectively.

building blocks of a fullerene. Similar to the second step, two hydrogen atoms are lost in the cyclization process, as H_2 with a reaction barrier of 2.2 eV. Because of the low barrier for the H_2 loss channel, the reaction pathway through $C_{26}H_{13}^+$ to $C_{26}H_{12}^+$ is energetically unfavorable. This is in line with the experimental observation that the $C_{26}H_{13}^+$ ($m/z = 325$) mass peak only is found with rather low signal strength.

To expand on this, the competing reaction pathways of the second and third dehydrogenated processes are shown in Figures 5(B) and 6(B), respectively. It is clear that the dehydrogenation of two hydrogen atoms may take place either on the same side of the carbon plane or on opposite sides. For $C_{26}H_{16}^+$ to $C_{26}H_{14}^+$, as shown in Figure 5(B), the two hydrogen atoms will be pushed to the same carbon plane, and then the hydrogen atoms are dissociated step by step. However, the reaction barrier for the first step is higher than the reaction pathway in Figure 5(A) by about 0.4 eV, so the pathway in Figure 5(A) is more energetically favorable. In a similar way, for the reaction of $C_{26}H_{14}^+$ to $C_{26}H_{12}^+$, as shown in Figure 6(B), the two hydrogen atoms will be pushed to a different carbon plane, and then the hydrogen atoms are dissociated step by step. As we can see, the barrier of the H + H dissociation pathway (Figure 6(B)) is higher than that of the H_2-releasing pathway in Figure 6(A) by about 0.5 eV, so the pathway in Figure 6(A) is more energetically favorable.

The photodissociation process from $C_{26}H_{18}^+$ to $C_{26}H_{12}^+$ outlined here is the cumulative result of dehydrogenation and isomerization steps, in which the 3D fluorene dimer cation becomes planar and then transforms into a bowl structure. As discussed above, the bonds that are present become more conjugated during this process. Figure 1 also shows the differential spectra. We have integrated the loss and gain peaks in the difference spectra without considering lower masses, and these nearly balance. Hence, H loss is the dominant channel and intramolecular dissociation into the two monomers is at most a very minor channel. This is somewhat surprising because DFT calculations yield that the CC bond energy linking the two monomers is only 1.4 eV, which is less than the sp^3 H loss channel (2.5 eV). Once a second covalent bond has been made linking the two monomers, the "dimer" has become planar and is in essence a large PAH. It is well known that H loss dominates C loss for large PAHs (Ekern et al. 1998; Zhen et al. 2014b; Castellanos et al. 2018; West et al. 2018). Negative balance for the fluorene trimer cation became clear in Figure 2. So, if there is an efficient dissociation of fluorene trimers and likely of other larger clusters, the efficiency of polymerization toward fragmentation needs to be considered. The dissociation of these large clusters by laser pulses likely generates different fluorene dimers.

For the fluorene trimer cation, the reaction pathway and energy barrier are very similar to but more complex than the dimer case. Here, we focus on the dehydrogenation reaction pathways shown in Figure 7, with the stable structures from $C_{39}H_{26}^+$, $m/z = 494$, to $C_{39}H_{20}^+$, $m/z = 488$. As discussed for the dimer cation, first the H atoms on the sp^3 hybridized carbon are dissociated to form $C_{39}H_{24}^+$. Subsequently, dehydrogenation and isomerization induce the formation of large PAHs ($C_{39}H_{22}^+$, part of the molecule becomes planar, while the other part starts to form a bowl). From $C_{39}H_{22}^+$, there are two different pathways of continued dehydrogenation: one

follows a bowl-forming process (1), the other retains the 3D structure of fluorene structures (2). Both end products have the same mass: $C_{39}H_{20}^{+}$, $m/z = 488$. The first process (1) is very similar to the photoinduced bowl-forming process described in detail for the fluorene dimer cation. Part of the resulting structure can be considered as a fragment of a functionalized fullerene. Unlike the quadrilateral-carbon ring attached on the fullerene surface obtained in Dunk et al. (2013), the three-carbon ring obtained here provides a possible starting point for new molecules in the ISM. In the second pathway, the resulting structure has a spiral-like geometry, which has potential for the growth of long PAH chains. We mention that six hydrogen atoms are lost in the dehydrogenation process from $C_{39}H_{26}^{+}$ to $C_{39}H_{20}^{+}$; due to the multiple aromatic/aliphatic bonds, the order of H loss might be sequential or simultaneous. This might be the reason why the dehydrogenation behavior of the fluorene trimer cation does not have the readily identifiable odd–even pattern seen in the dimer case (or for other previously studied PAHs). In addition, in Figure 2, C_2H_2/CH loss and dehydrogenation photoproducts are observed in the range $m/z = 448$–484. We observe masses corresponding to $C_{38}H_m^{+}$ and $C_{37}H_n^{+}$ with $m, n = [17, 25]$. We emphasize that these ions are not fully dehydrogenated and no pure carbon clusters are produced.

5. Astronomical Implications

In our experiments, we employ an ion trap to isolate the covalently bonded clusters and study their subsequent evolution under irradiation. This evolution is driven by the high internal energy attained by photon absorption. Rapid internal conversion followed by intramolecular vibrational redistribution leaves the species highly vibrationally excited in the ground electronic state (Tielens 2008; Joblin & Tielens 2011). Cooling occurs through a competition between vibrational emission in the IR and fragmentation (mainly H loss for these species) (Montillaud et al. 2013). While the details of these processes (e.g., energy barriers, IR relaxation rates) will depend on the charge state, the evolution of neutrals will parallel that of ions and hence our experiments will be of general relevance. Further experiments will be needed to address the details of the evolution of neutral clusters.

As discussed in the introduction, observational and theoretical studies support the presence of PAH clusters in space (Rapacioli et al. 2005; Rhee et al. 2007). Observations show that some 3% of the elemental carbon is locked up in PAH clusters deep in PDRs, such as NGC 7023 (Rapacioli et al. 2005; Tielens 2008). For comparison, C_{60} locks up less than 2×10^{-4} of the elemental carbon in NGC 7023 and some 10^{-3} in the diffuse ISM (Campbell et al. 2016; Berné et al. 2017). Hence, from the point of view of abundance, the formation of fullerenes through photoprocessing of PAH clusters is feasible. In principle, as outlined in Zhen et al. (2018), photolysis of PAH clusters could lead to large PAHs, which could then photochemically evolve to fullerene in a top-down fashion (Zhen et al. 2014a). Whether processing of small PAHs with pentagons can facilitate the formation of fullerenes as suggested by the experiments and calculations presented here depends on whether interstellar PAHs contain pentagons.

It is not known whether interstellar PAHs have pentagons in their structure. There is spectroscopic support for the presence of carbonyl groups in the PAH family (Tielens 2008), and we have shown in a previous study that PAH-quinones will readily evolve photochemically toward pentagon-containing structures before they start losing H atoms (Chen et al. 2018). Laboratory studies have revealed that quinones are readily made by photolysis of PAHs in ices (Bernstein et al. 2003).

Experiments and theory have shown that fullerenes could form from the photochemical processing of large PAHs (Berné & Tielens 2012; Zhen et al. 2014a). In this scenario, large PAHs originate from the ejecta of dying stars and are then broken down by UV photolysis in the ISM into more stable species, such as C_{60}. In this study we have demonstrated that the photochemical evolution of charged PAH clusters, containing pentagon structures, leads in a natural way to curvature, which is a first and essential step toward fullerene formation. It also opens up bottom-up chemical scenarios where small PAHs grow through cluster formation and photolysis to fullerenes, bypassing the large PAH intermediaries. This results adds to a few other studies that addressed the formation of non-planar PAHs, such as through the photochemical processing of functionalized PAHs (de Haas et al. 2017; Chen et al. 2018). While full analysis has to await kinetic studies, we emphasize that the reservoir of PAH clusters is ample to supply C_{60} in the ISM. Moreover, caged C_{60}, as well as larger fullerenes, is expected to be much more stable than PAH clusters in the ISM (Berné et al. 2015).

H loss only happens after absorption of photons that raise the internal energy to $\sim$10−20 eV depending on the size of PAHs (Zhen et al. 2014b). The same holds for the ISM. PAHs of the size that is relevant in space require multiphoton absorption before fragmentation will occur (Andrews et al. 2015; Berné et al. 2015). We stress here that the derived energy barriers (from 1.5 eV up to 3.0 eV) for all the dehydrogenation and isomerization steps are smaller than the energy barrier for dehydrogenation of pure PAHs ($\sim$4.5 eV) (Chen et al. 2015). So, as in H I regions ($5.0 < E < 13.6$ eV), the energy of a single photon is capable of photodissociating small PAH clusters (e.g., a fluorene dimer cluster with 3.0 eV energy barrier). For clusters consisting of larger PAHs, absorption of multiple photons is required. While this will be a rare process, it can still be of importance given the long timescales involved in evolution of the ISM (Montillaud & Joblin 2014).

The present study shows results on a prototypical laboratory example. As stated before, the presence of PAH cluster ions in space is still under debate. The detection of a specific PAH would be a major step forward, and this links again to the work presented here. The non-planar species will be polar and should be detectable by radio astronomy, because the bowl-forming introduces a dipole moment. Emission by such species will contribute to the anomalous microwave emission (Lagache 2003; Ysard & Verstraete 2010). In view of the large partition function of such large, non-planar molecules, unambiguous detection of individual species will be very challenging. First attempts in this direction, searching for the small, corannulene bowl, were unsuccessful (Lovas et al. 2005; Pilleri et al. 2009). With the bowling concept introduced for the bisanthenequinone cation (Chen et al. 2018) and extended in this study for fluorene clusters, a new class of PAH derivatives may become within range.

6. Conclusions

Combining experiments with quantum chemical calculations, we have presented evidence for the dehydrogenation and

Table 1
Hydrogen Dissociation Energies with Different Functionals Using the 6-311++G** Basis Set

DFTs	First H	Second H
B3LYP	2.337	2.614
B3LYP-D3	2.456	2.695
M06HF	2.198	3.104
PBE	2.330	2.522

Note. The zero-point vibrational energy has also been taken into account (unit: eV).

isomerization process of charged covalently bonded clusters of fluorene dimers and trimers under laser irradiation, which shows that after H loss the clusters will isomerize and aromatize, leading to bowled and curved structures. Under the assumption that PAH cluster ions play an important role in the ISM, this process may offer a way to form species that might act as building blocks of cages and fullerenes.

This work is supported by the Fundamental Research Funds for the Central Universities of China and by the National Science Foundation of China (NSFC, grant No. 11743004, grant No. 11421303, and grant No. 11590782). Studies of interstellar chemistry at Leiden Observatory are supported through advanced-ERC grant 246976 from the European Research Council, through a grant by the Netherlands Organisation for Scientific Research (NWO) as part of the Dutch Astrochemistry Network, and through the Spinoza premie. H.L. and A.T. acknowledge the European Union (EU) and Horizon 2020 funding awarded under the Marie Sklodowska-Curie action to the EUROPAH consortium, grant No. 722346. Y.S. thanks the support of Science and Technology Development Program of Henan province (172102310164). T.C. acknowledges Swedish Research Council (Contract No. 2015-06501) and Swedish National Infrastructure for Computing (Project No. SNIC 2018/5-8).

Appendix A
Details of the Theoretical Calculation

Our theoretical calculations are carried out using DFT. The dissociation energies, minimum energies, and transition state energies presented in this work are calculated using the hybrid functional B3LYP (Becke 1992; Lee et al. 1988) as implemented in the Gaussian 16 program (Frisch et al. 2016). All structures are optimized using the 6-311++G(d,p) basis set. The vibrational frequencies are calculated for the optimized geometries to verify that these correspond to minima or first-order saddle points (transition states) on the potential energy surface. We have taken the zero-point vibrational energy into account.

In addition, to valid B3LYP, we took the reactions from $C_{26}H_{18}^{+}$ to $C_{26}H_{16}^{+}$ (losing hydrogen atoms step by step) as an example to make a comparison of the calculation results for various functionals, namely B3LYP-D3 (dispersion correction), PBE (pure functional), and M06HF (hybrid meta-GGA functional). The latter two functionals have been demonstrated to be able to give an accurate description of hemolytic bond-breaking (O'Reilly & Karton 2016). Table 1 shows the hydrogen dissociation energies obtained with different functionals. Clearly, B3LYP predicts similar results to PBE and B3LYP-D3, indicating that the typical problem of hemolytic bond-breaking is not important in the current charged species.

Appendix B
DFT Studies of the Structure of the Fluorene Dimer and Trimer

Focusing on the most abundant dimer and trimer ions ($C_{26}H_{18}^{+}$ and $C_{39}H_{26}^{+}$), we conclude that the complexation from monomer to dimer or trimer occurs on the sp^3 hybridized carbon of the fluorene molecules (Lang et al. 2013). Since the density of natural and ionic fluorene is higher in the ionization zone of i-PoP, a possible formation pathway of dimer and trimer fluorene cations could be the interaction between dehydrogenated neutral and charged fluorenes. Furthermore, loss of H from the fluorene cation has a dissociation energy of only ~2.3 eV, which means that $C_{13}H_9^{+}$ is more abundant than $C_{13}H_{10}^{+}$. Additionally, considering the fact that hydrogen dissociates from sp^3 hybridized carbon atoms much more easily than from an aromatic ring, we expect the structure of $C_{26}H_{18}^{+}$ to be bonded dimers (West et al. 2018). Alternatively, it has been shown that ionization of van der Waals clusters of acetylene results in barrierless formation of covalently bonded larger species (Stein et al. 2017), and a similar process may be at work here. Our theoretical study shows that the dimer structure consists of two mono-fluorenes connected by a C−C single bond (as $[C_{13}H_9{-}C_{13}H_9]^{+}$), where two sp^3 hybridized carbon atoms have one C–H bond each; the trimer structure is that of three mono-fluorenes connected by two C−C single bonds (as $[C_{13}H_9{-}C_{13}H_8{-}C_{13}H_9]^{+}$), where three sp^3 hybridized carbon atoms have one C–H bond each. The optimized carbon skeletons of these fluorene units are not in the same plane, but form a three-dimensional structure. The dimer and trimer radical cations contain aliphatic units, in agreement with our interpretation of the experimental photodehydrogenation results.

ORCID iDs

Tao Chen https://orcid.org/0000-0003-4145-4300
Harold Linnartz https://orcid.org/0000-0002-8322-3538

References

Allamandola, L. J., Tielens, A. G. G. M., & Barker, J. R. 1989, ApJS, 71, 733
Andrews, H., Boersma, C., Werner, M. W., et al. 2015, ApJ, 807, 99
Becke, A. D. 1992, JChPh, 96, 2155
Berné, O., Cox, N. L. J., Mulas, G., & Joblin, C. 2017, A&A, 605, L1
Berné, O., Joblin, C., Deville, Y., et al. 2007, A&A, 469, 575
Berné, O., Montillaud, J., & Joblin, C. 2015, A&A, 577, A133
Berné, O., & Tielens, A. G. G. M. 2012, PNAS, 109, 401
Bernstein, M. P., Moore, H. M., & Elsila, J. E. 2003, ApJL, 582, L25
Cami, J., Bernard-Salas, J., Peeters, E., & Malek, S. E. 2010, Sci, 329, 1180
Campbell, E. K., Holz, M., Gerlich, D., & Maier, J. P. 2015, Natur, 523, 322
Campbell, E. K., Holz, M., Maier, J. P., et al. 2016, ApJ, 822, 17
Castellanos, P., Candian, A., Zhen, J., Linnartz, H., & Tielens, A. G. G. M. 2018, A&A, 616, A166
Chen, T., Gatchell, M., Stockett, M. H., et al. 2015, JChPh, 142, 144305
Chen, T., Zhen, J., Wang, Y., Linnartz, H., & Tielens, A. G. G. M. 2018, CPL, 692, 298
Chuvilin, A., Kaiser, U., Bichoutskaia, E., Besley, N. A., & Khlobystov, A. N. 2010, NatCh, 2, 450
Cordiner, M. A., Cox, N. L. J., Lallement, R., et al. 2017, ApJL, 843, L2
de Haas, A. J., Oomens, J., & Bouwman, J. 2017, PCCP, 19, 2974
Dunk, P. W., Adjizian, J. J., Kaiser, N. K., et al. 2013, PNAS, 110, 18081
Ekern, S. P., Marshall, A. G., Szczepanski, J., & Vala, M. 1998, JPCA, 102, 3498

Frisch, M. J., et al. 2016, Gaussian 16 Revision e.01 (Wallingford, CT: Gaussian Inc.)
Gatchell, M., Delaunay, R., & Maclot, S. 2015, JPhCS, 583, 012011
Gatchell, M., & Zettergren, H. 2016, JPhB, 49, 162001
Genzel, R., Lutz, D., Sturm, E., et al. 1998, ApJ, 498, 597
Gredel, R., Carpentier, Y., Rouillé, G., et al. 2011, A&A, 530, A26
Joblin, C., & Tielens, A. G. G. M. 2011, EAS Pub. Ser. 46, PAHs and the Universe: A Symp. to Celebrate the 25th Anniversary of the PAH Hypothesis (Les Ulis: EAS)
Jolibois, F., Klotz, A., Gadéa, F. X., & Joblin, C. 2005, A&A, 444, 629
Lagache, G. 2003, A&A, 405, 813
Lang, M., Holzmeier, F., Fischer, I, et al. 2013, JPCA, 117, 5260
Lee, C., Yang, W., & Parr, R. G. 1988, PhReB, 37, 785
Le Page, V., Snow, T. P., & Bierbaum, V. M. 2001, ApJS, 132, 233
Lovas, F. J., McMahon, R. J., Grabow, J. U., et al. 2005, J. Am. Chem. Soc, 127, 4345
Micelotta, E. R., Jones, A. P., Cami, J., et al. 2012, ApJ, 761, 35
Montillaud, J., & Joblin, C. 2014, A&A, 567, A45
Montillaud, J., Joblin, C., & Toublanc, D. 2013, A&A, 552, A15
O'Reilly, R. J., & Karton, F. 2016, IJQC, 116, 52
Pietrucci, F., & Andreoni, W. 2014, J. Chem. Theory Comput., 10, 913
Pilleri, P., Herberth, D., Giesen, T. F., et al. 2009, MNRAS, 397, 1053
Puget, J. L., & Leger, A. 1989, ARA&A, 27, 161
Rapacioli, M., Calvo, F., Joblin, C., et al. 2006, A&A, 460, 519
Rapacioli, M., Joblin, C., & Boissel, P. 2005, A&A, 429, 193
Rhee, Y. M., Lee, T. J., Gudipati, M. S., Allamandola, L. J., & Head-Gordon, M. 2007, PNAS, 104, 5274
Richter, H., Granata, S., Green, W. H., & Howard, J. B. 2005, Proc. Combust. Inst., 30, 1397
Richter, H., & Howard, J. B. 2000, PrECS, 26, 565
Salama, F., Bakes, E. L. O., Allamandola, L. J., & Tielens, A. G. G. M. 1996, ApJ, 458, 621
Sellgren, K. 1984, ApJ, 277, 623
Sellgren, K., Wener, M. W., Ingalls, J. G., et al. 2010, ApJ, 722, 54
Sephton, M. A. 2002, Natural Product Report, 19, 292
Stein, T., Bandyopadhyay, B., Troy, T. P., et al. 2017, PNAS, 114, E4125
Tielens, A. G. G. M. 2008, ARA&A, 46, 289
Tielens, A. G. G. M. 2013, RvMP, 85, 1021
Trinquier, G., Simon, A., Rapacioli, M., & Gadéa, F. X. 2017, MolAs, 7, 37
Vijh, U. P., Witt, A. N., & Gordon, K. D. 2004, ApJL, 606, L65
Walker, G. A. H., Bohlender, D. A., Maier, J. P., & Campbell, E. K. 2015, ApJL, 812, L8
West, B., Castillo, S. R., Sit, A., et al. 2018, PCCP, 20, 7195
Ysard, N., & Verstraete, L. 2010, A&A, 509, A12
Zettergren, H., Rousseau, P., Wang, Y., et al. 2013, PRL, 110, 185501
Zhen, J., Castellanos, P., Paardekooper, D. M., Linnartz, H., & Tielens, A. G. G. M. 2014a, ApJL, 797, L30
Zhen, J., Chen, T., & Tielens, A. G. G. M. 2018, ApJ, 863, 128
Zhen, J., Paardekooper, D. M., Candian, A., Linnartz, H., & Tielens, A. G. G. M. 2014b, CPL, 592, 211